Progress Report – YEAR 2

Title: *Interactions between agricultural development in southwestern US / northwestern Mexico and the North American Monsoon with a focus on water resources*

Project Duration: 1 April 2004 – 31 March 2007

Name of PI: Roni Avissar

Institution: Duke University – Department of Civil and Environmental Engineering

Introduction:

Southwestern US and northwestern Mexico are characterized by their arid to semiarid climate and, consequently, anthropogenic activity in that region is highly dependent upon water resources. Understanding the water cycle (which in turn can be affected by anthropogenic activity as well as natural phenomena) and its predictability are key factors for water resources management and, therefore, the socio-economical development and sustainability of that region. The hydroclimate of that region is significantly affected by the North American Monsoon (NAM), which supplies most of the moisture source from the Gulf of California, the Eastern Pacific and the Gulf of Mexico. But population growth and agricultural and urban development is significantly changing the regional landscape, including land cover and soil moisture. Therefore, complex ocean-land-atmosphere interactions may take place in that region and possibly at other locations in North America that are normally affected by the NAM. Three main rivers are originated in that region: the Sonora, the Yaqui and the Mayo. They supply the water to the major urban and agricultural developments in the area.

Project Goals:

The objective of the research proposed here is to study in details the various interactions in the ocean-land-atmosphere system in that region, with a special interest in the NAM system. Focusing on water resources applications, we concentrate on precipitation and river discharge in the Sonora, Yaqui and Mayo river basins. The hydrometeorology of that region is being simulated at a very-high resolution (1 x 1 km^2 horizontal grid size) with the Regional Atmospheric Modeling System (RAMS), for which the hydrology module is being improved to better simulate river discharge in this region. RAMS has been upgraded in its latest version (Version 6.0) to include a new coordinate system especially designed to improve simulations in complex terrain and it also benefits from the regional reanalysis available since Fall 2003 to force its lateral boundary.

Method:

To address the following five scientific questions: (1) is the current generation of very-high resolution, state-of-the-art mesoscale models capable of simulating the evolution of the NAM in southwestern US / northwestern Mexico; (2) what are the parameters that affect the evolution of the NAM in that region; (3) are these parameters useful for

improving the predictability of the NAM and the discharge of the Sonora, Yaqui, and Mayo rivers; (4) has the development of agriculture in that region affected river discharge and the evolution of the NAM through ocean-land-atmosphere interactions and feedbacks; and (5) what is the sensitivity of that region to further rural and urban development in that region; three major tasks are being performed: (1) an evaluation of RAMS performance (with an emphasis on precipitation and river discharge) when used at very-high resolution in that region; (2) a sensitivity analysis of the relative importance of various parameters susceptible of impacting precipitation and river discharge in that region (i.e., sea-surface temperature, soil moisture, land cover) and their interactions with the NAM; and (3) an analysis of the NAM evolution and variability as affected by various scenarios of agricultural and urban development in that region. Special attention will be paid to monthly to interannual variability and how the results of these three tasks are affected by El Niño and La Niña events.

Combining the results from these three tasks, we expect to provide new insights and a much clearer understanding of (1) the evolution of the NAM system and its variations; (2) the response of the warm season atmospheric circulation and precipitation patterns to slowly varying boundary conditions (i.e., SST, soil moisture and vegetation cover); and (3) the role of the NAM system in the regional water cycle and climate variability. Finally, this project will contribute to improving the monthly to interannual prediction of the NAM system and regional water resources and, therefore, it addresses key elements of the PACS/GAPP North American warm season precipitation initiative.

Results and Accomplishments (Year 2: 04/01/2005 – 12/31/2005)[1]:

A. Precipitation

a. Data Analysis

For this study, we limit our analysis to public datasets reported in the literature that have passed quality procedures. A total of 22 datasets (Table I) based on precipitation measurements by rain gauge, remote sensing (passive and active sensors; Geosynchronous- and Polar-orbiting satellites), merged products, and modeling products are considered. The 8-year period from 1997 to 2004 was chosen for the evaluation. This period includes flood and drought events associated with El Niño and La Niña events. This specific period also allow us to study the intraseasonal and interannual variability of precipitation in the NAM region.

The spatial and temporal comparisons between the databases are based on basic statistical moments and the application of Empirical Orthogonal Functions (EOF). EOF or Principal Components Analysis (PCA) take the space-time matrices (cells *vs* months) to derive matrices of covariances. Then they solve their eigenvalues. For our purpose, the resulting eigenvectors (known as spatial EOF or loading functions) indicate the spatial patterns associated with the spatial distribution of precipitation. The evolution of these patterns is represented by the temporal EOF or expansion coefficients. Temporal EOF are

[1] Please see my First Year Report for the research activity conducted during the first year of the project, which provides all necessary background for the results described here.

used to determine the fraction of the total variance explained by each mode, which define the main spatial and temporal EOF to be evaluated. Janowiak (1998) and Yin et al (2004) used PCA to compare datasets (GR *vs* GPCP, and GPCP *vs* CMAP, respectively) on a global basis, obtaining from the first two modes the signal produced by El Niño-La Niña. Here, the EOF are used to capture similar signals and those that contribute to the complexity of the core domain of NAM.

Table I: Precipitation datasets used for our study

		Time Coverage	Time Resol	Spatial Cov	Spatial Res	Technique	Orbit	Units	Precip SUMEX mm/day	Rate NAM mm/day
1*	**USMEX**	1948-curr	Dy	Reg	1.0	Rain Gauge		mm/day	1.93	0.94
2	**PREC or NCEP**	1979-curr	Mo	Global	2.5	Rain Gauge		mm/day	2.27	0.89
3	**Pms**	1979-curr	Mo	Global	2.5	Multi-satellite		mm/day	2.32	1.38
4	**Psc**	1987-curr	Mo	Global	2.5	PasMW-comp	Sun-synchronous Near Polar	mm/day	2.73	1.73
5	**Pss**	1987-curr	Mo	Global	2.5	PasMW-sctt	Sun-synchronous Near Polar	mm/day	2.73	1.73
6	**Ptv**	1987-curr	Mo	Global	2.5	PasMW-TOVS		mm/day	2.2	1.26
7	**SSMI**	1987-2004	Mo	Global	1.0	Passive MW	Sun-synchronous Near Polar	mm/mn	2.78	1.87
8	**TRMM 3A12**	1997(12)-curr	Mo	Tropical	0.5	Passive MW	Geosynchro	mm/hr	2.67	1.89
9	**TRMM 3A25**	1997(12)-curr	Mo	Tropical	0.5	Radar	Geosynchro	mm/hr	2.47	2.02
10	**TRMM 3A25b**	1997(12)-curr	Mo	Tropical	5.0	Radar	Geosynchro	mm/hr	2.43	1.38
11	**TRMM 3B31**	1997(12)-curr	Mo	Tropical	5.0	Pasive MW+Radar	Geosynchro	mm/hr	2.95	1.68
12*	**Global Reanal.**	1979-curr	Dy	Global	2.5	Modeling		mm/sec	3.52	1.75
13*	**Reg. Reanal.**	1948-curr	3Hr	Reg	0.3	Modeling		mm/sec	1.84	0.83
14*	**TRMM 3B42**	1997(12)-curr	3-Hr	Tropical	0.25	Merged		mm/hr	2.32	0.92
15	**TRMM 3B43**	1997(12)-curr	Mo	Tropical	0.25	Merged		mm/hr	2.40	0.95
16*	**GPI**	1987-curr	Dy	Global	1.0	IR/VIS	Geostatio	mm/day	2.89	2.15
17	**AGPI**	1987-curr	Mo	Global	1.0			mm/day	2.21	0.31
18	**OPI**	1979-2000	Mo	Global	2.5	Scanning Radiometer IR/VIS	Sun-synchronous Polar	mm/day	2.44	1.05
19	**CMAP**	1979-curr	Mo	Global	2.5	Merged		mm/day	2.20	0.85
20	**CMAPe**	1979-curr	Mo	Global	2.5	Merged		mm/day	2.19	0.85
21*	**GPCP 1DD**	1979-curr	Dy	Global	1	Merged		mm/day	2.41	0.96
22	**GPCP V.2**	1979-curr	Mo	Global	2.5	Merged		mm/day	2.33	0.96

The homogenization of the datasets involves the use of aggregation and disaggregation techniques (Fiorino, 2002) to determine whether or not information is lost due to increase or decrease of resolution (Fig. 1). To determine the effect of the aggregation technique and the spatial resolution on the spatiotemporal precipitation variability in the SUS-MEX domain, three-aggregation/disaggregation techniques are considered (third order Bessel, Bilinear, and Box Averaging interpolation) at four spatial resolutions (0.25, 0.5, 1.0 and 2.5^{o}) on a monthly basis. The selection of the aggregation/disaggregation technique and resolution that will be retained will be based on the comparison of the fractions of the variability explained by the different temporal EOF.

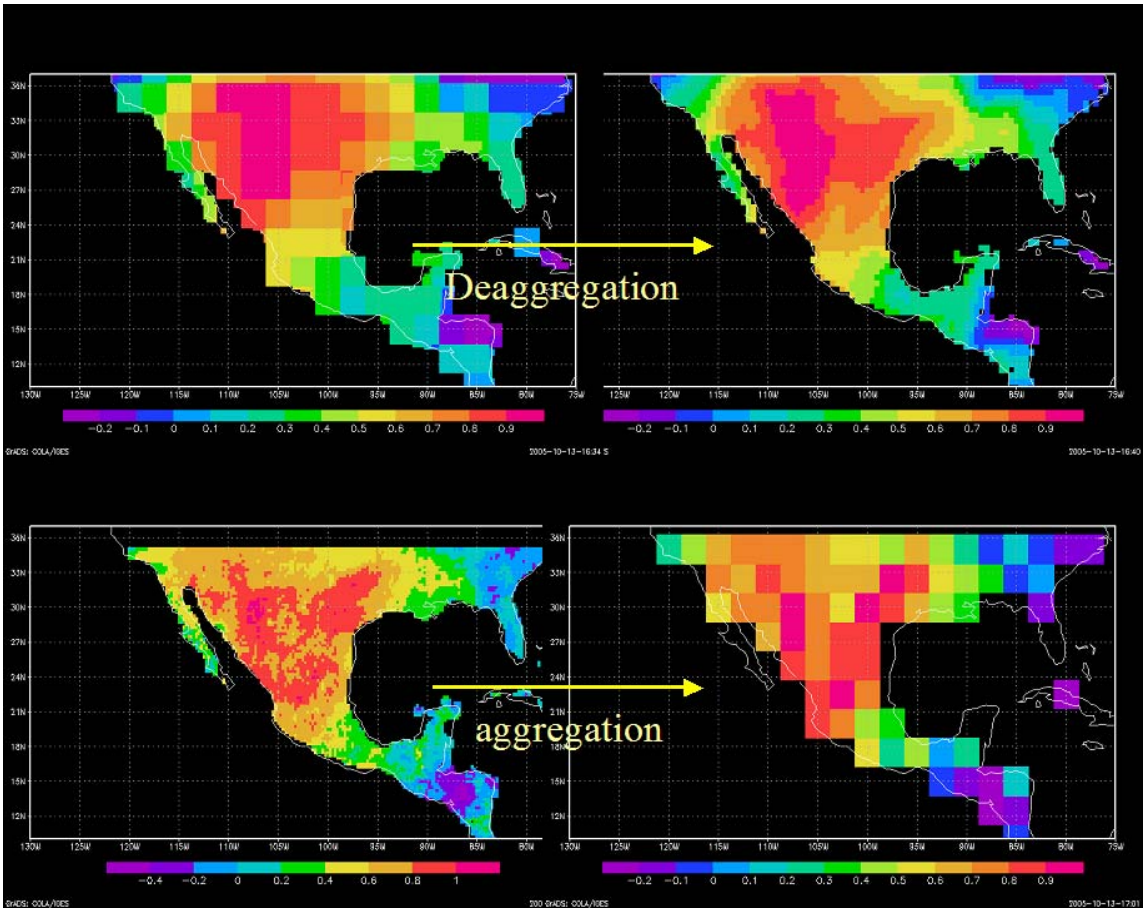

Figure 1: *Precipitation (mm/day) aggregation-disaggregation for two different merged products with low (top – GPCP V.2) and high (bottom – 3B43 TRMM) initial resolution.*

The main pattern of variability, mostly seen in the first and second EOF, is expected to be associated with the variability of the geophysical variables such as topography, vegetation, and soil moisture. Topography is obtained from the 1-km USGS dataset. Vegetation is the same as that used in the Regional Reanalysis (RR), which has a 0.3^{o} resolution. Soil moisture data is obtained from the UW 0.12^{o} resolution dataset. While topography and vegetation are considered constant with time, soil moisture varies and is compared on a monthly basis. All the datasets are regridded to a resolution of 0.25^{o} using

the technique described above. The correlation coefficients are used to compare the precipitation variability with the variability of variables such as the Southern Oscillation Index, vegetation cover, topography, and soil moisture.

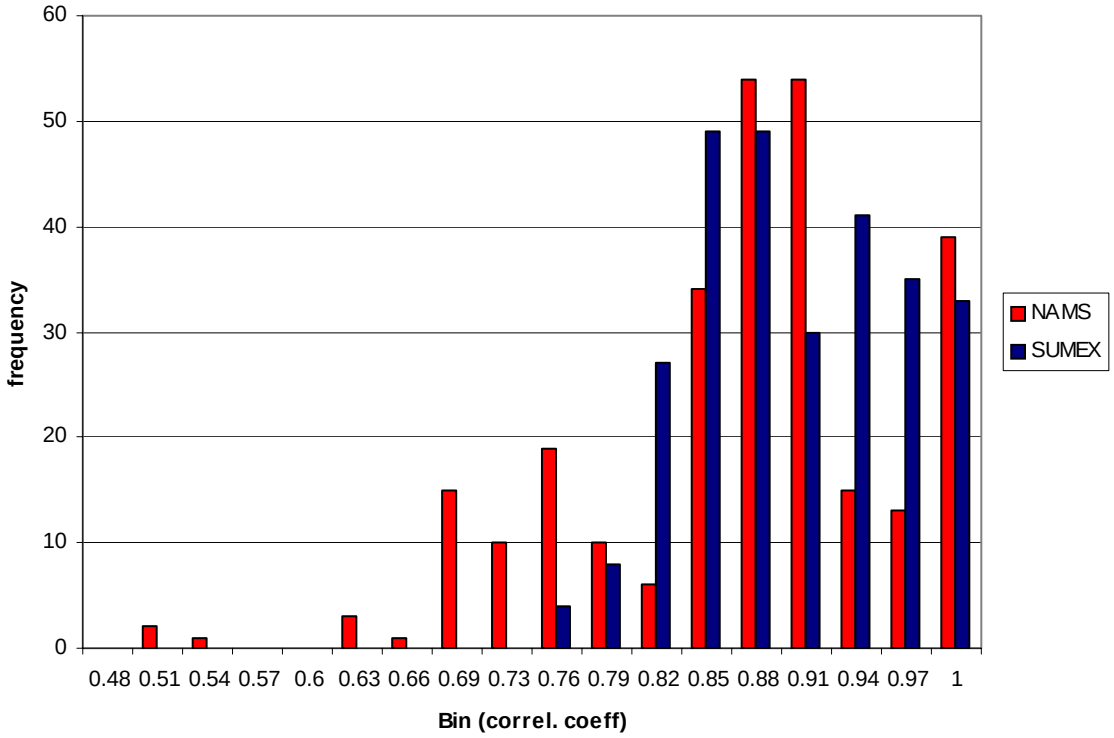

Figure 2: *Histogram of correlation coefficients between the 22 precipitation datasets used in our study and summarized in Table 1.*

The correlation coefficients (CC) obtained between the precipitation datasets (summarized Table 1) are presented in Fig. 2. Most CC are between 0.84 and 0.9. CC below 0.7 are just seen in NAM and represent the correlations between global reanalysis, GPI, AGPI, and 3B41.

Datasets were regrouped into a few categories: rain gauge (GG), remote sensing (SENS), simple merging (SIM), complex merging (COM), and modeling (MOD) products. The spatial distribution of precipitation in the SUMEX region shows that SENS, COM, and GG products tend to be similar for the 1997-2004 period (Fig. 3). In the NAM region, all the datasets tend to reproduce the same spatial pattern of precipitation with some changes in the northwestern precipitation highs (Fig. 4). In both domains, measuring techniques behave similarly in high-precipitation areas (>3mm/day). But this behavior is not similar to what is observed in low-precipitation areas, where GG, COM, and SENS products record a dry area that extends from the mid Southern USA to the Southern states of the Mexican Pacific Coast. This low-precipitation pattern recorded in the SIM and MOD (and, to a lesser extent, in SENS) products differs from the GG product. Precipitation rates above 1mm/day along the central portion of the Sierra Madre Occidental, from the Pacific Coast of Central Mexico to Southeastern USA, suggest that

there is a poor distribution of rain gauges in this steep-topography area. Consequently, merged products such as CMAP and GPCP, whose algorithms integrate rain gauge measurements, are likely to be also affected by the low distribution of instruments.

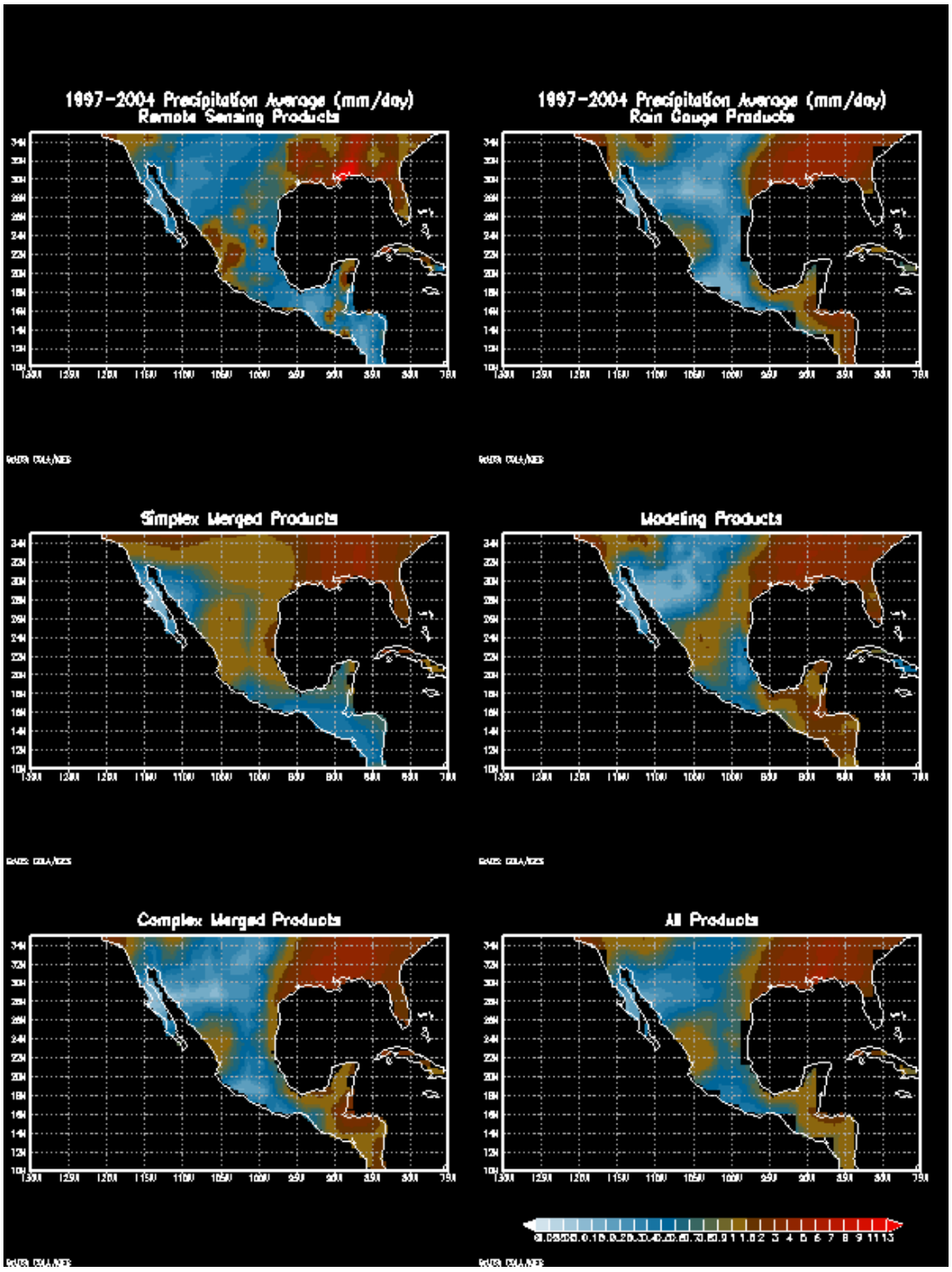

Figure 3: *Precipitation averages obtained with different measurement techniques in the SUMEX domain from 1997 to 2004.*

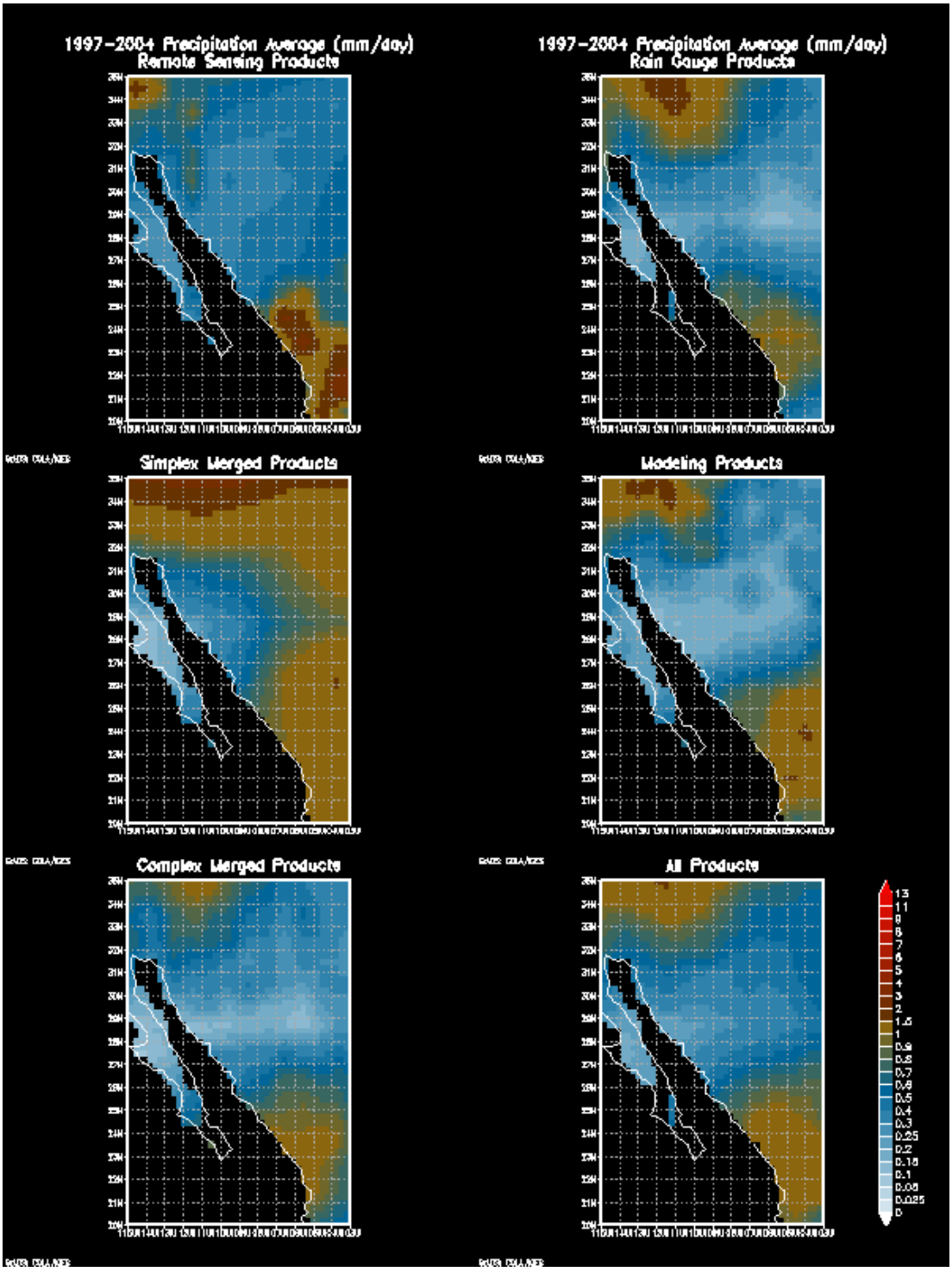

Figure 4: *Precipitation averages obtained with different measurement techniques in the NAM domain from 1997 to 2004.*

Figure 5 shows the spatial mean, standard deviation, and coefficient of variation for the SUMEX and the NAM domains. These statistics are obtained from 18 datasets including SENS (n=4), SIM (n=4), COM (n=4), GG (n=3), and MOD (n=3). In the SUMEX

domain, the standard deviation of precipitation has two main features: High precipitation is obtained in the US coastal area of the Gulf of Mexico, Southeastern Mexico and Central America; And low precipitation is seen in the NAM-affected region.

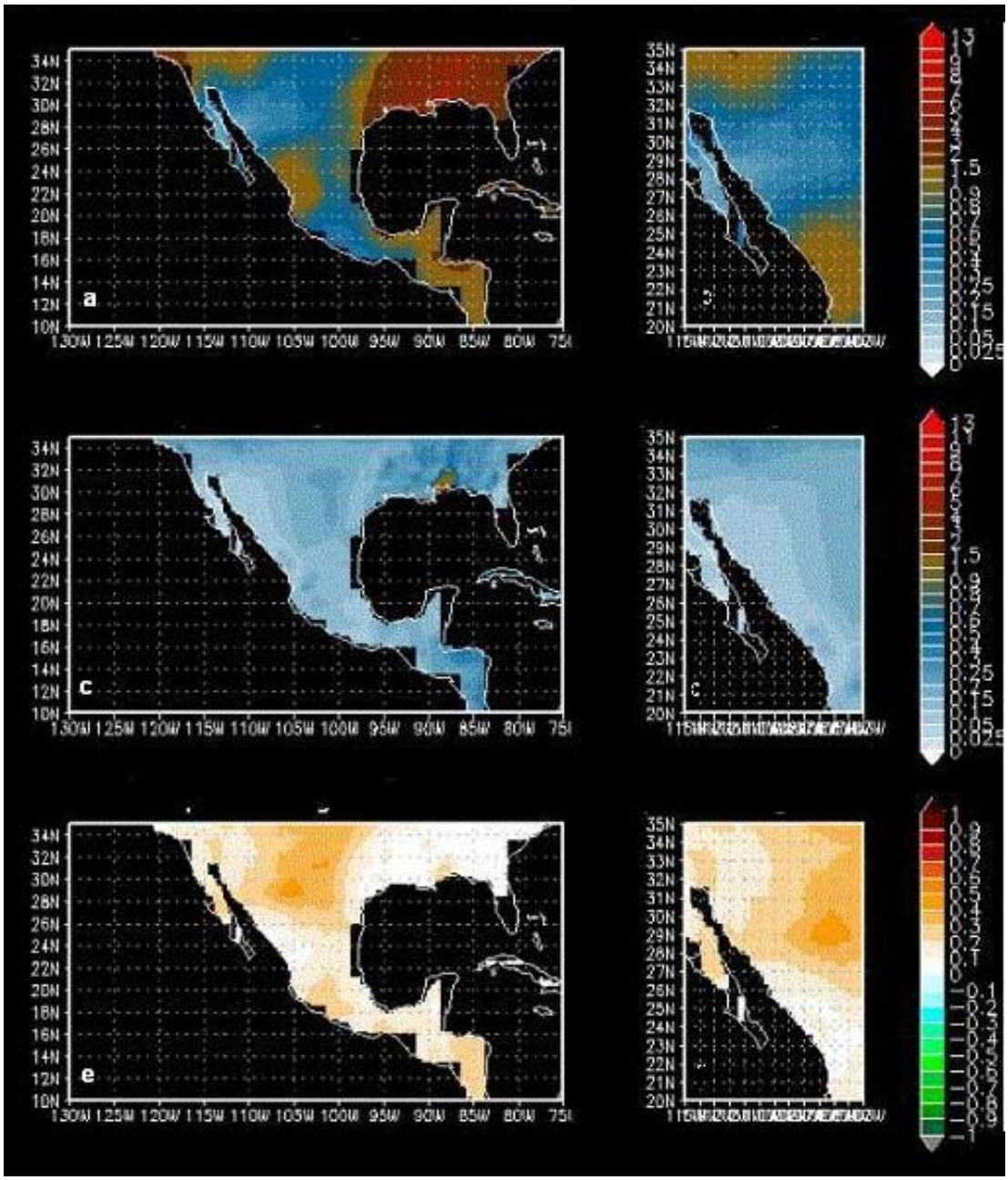

Figure 5: *Mean (mm/day; a and b), standard deviation (mm/day; c and d), and coefficient of variation (d and e) obtained from all the datasets (n=18).*

The coefficient of variation highlights those areas where the uncertainty is not only attributed to the magnitude of the precipitation but also to the deficiency of the measurement techniques. The central part of the Southern USA – Northern Mexico has a

coefficient of variation of 0.4, which represents 40% of the mean value. The low standard deviation area along the coast of the Gulf of California is not evident in the coefficient of variation, which shows a gradient toward high altitudes but does not follow the topography of the Sierra Madre Occidental.

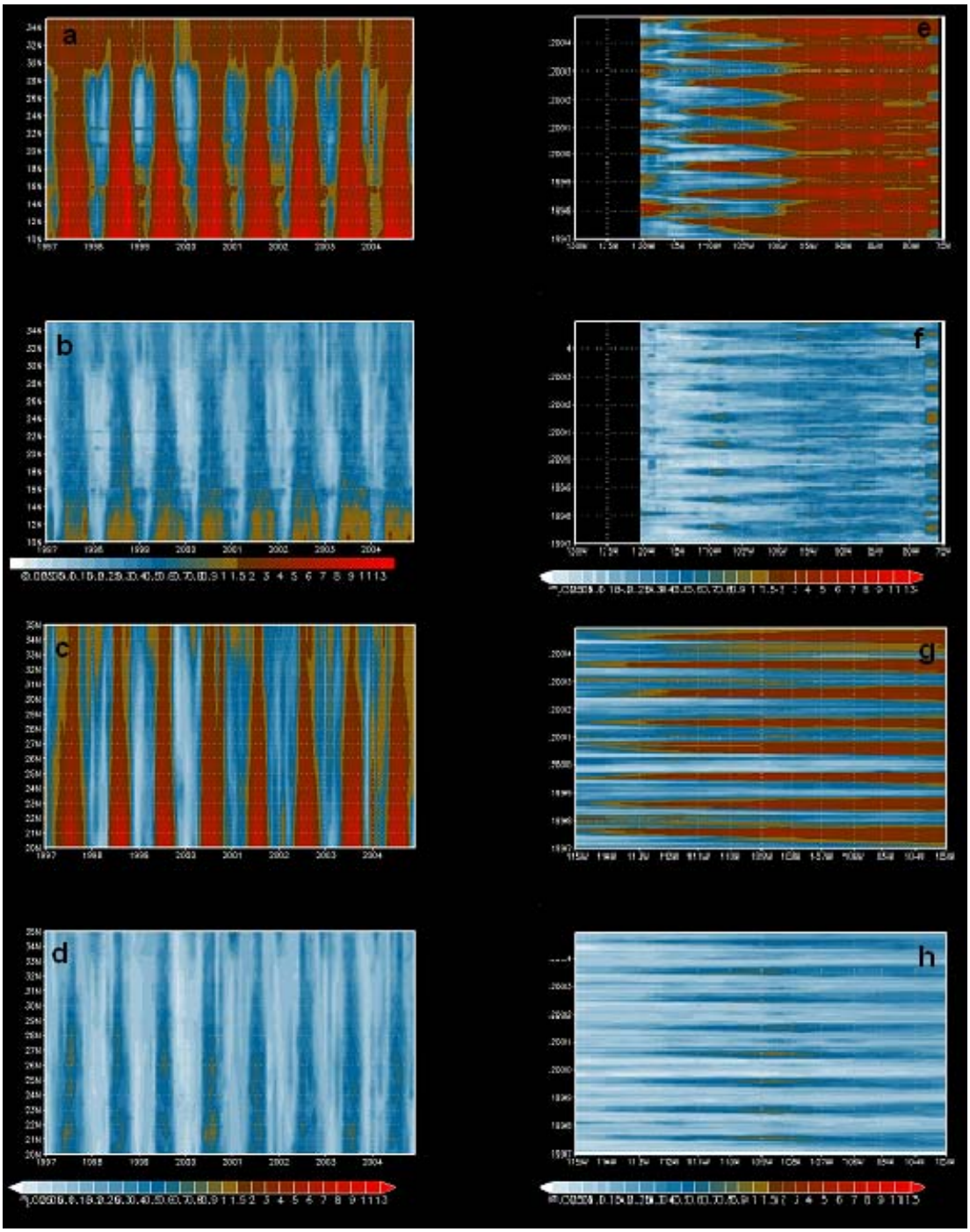

Figure 6: *Zonal (a, c) and meridional (e, g) means, and zonal (b, d) and meridional (f, h) standard deviations in SUMEX (a, b, e, f) and NAM (c, d, g, h) obtained from all datasets (n=18).*

The zonal mean and standard deviation depict three main features (Fig. 6). The first one is the bimodal precipitation highs between latitude 10°N and 28°N. The associated summer precipitation low is known as the mid-summer drought and is characteristic of the central and southern parts of the Mexican territory. The second one is the single peak of high summer precipitation above latitude 20°N, which indicates the NAM. The high zonal standard deviation in the SUMEX domain during the entire year contrasts with the low one obtained in the NAM domain. This difference is due to the persistent interannual variability of the monsoonal precipitation and the highly variable interannual and intraseasonal patterns of precipitation in the SUMEX domain. The third feature is the high precipitation obtained in Southeastern USA, Southeastern Mexico and Central America during the entire year. The coefficients of variation, however, are considerably higher in Southeastern Mexico and Central America. This is likely due to the data reliability in that region.

The meridional mean precipitation shows similar interannual variability, decreasing gradually from longitude 80°W to longitude 115°W. The precipitation peak varies almost every year (Fig. 6). For example, in 1997 it occurs toward the end of the year, while in 1998, 1999, 2001 and 2002 it occurs during the summer. The high precipitation observed between 115°W and 121°W are due to the Southern California precipitation patterns, which are associated with strong El Niño (1997-1998) and La Niña (1998-1999) events. The main feature in the meridional standard deviation of precipitation is its high value between longitudes 105°W and 110°W during the summer, which is likely related to deficiencies in the GG and COM products in steep topographies.

The mean of all precipitation products for SUMEX and NAM is 2.48 and 1.37, respectively. The coefficient of variation for NAM is twice that for SUMEX (14%). This points out high uncertainty in precipitation patterns over small domains. In SUMEX, precipitation is low during the winter and spring months, but high during the summer. This pattern is also seen in the standard deviation, which tends to be higher during the high precipitation season. During El Niño years, the difference between the maximum and the mean is larger than during La Niña years. But the intraseasonal variability in NAM during the 1997-2004 period is different that that observed in SUMEX (Fig. 7).

The Empirical Orthogonal Function (EOF) analysis is applied to the precipitation datasets. The Barnet (1998) approach, which consists of integrating all the datasets into one analysis that summarizes the main spatial patterns of precipitation and their temporal variability was adopted here. The resulting temporal EOF for NAM highlights patterns of variability not clearly observed in the spatiotemporal analysis described above. For example, the first, second, and third EOF together explain 80% of the variability (Fig. 8). The spatial EOF are compared to the spatial patterns of the coefficient of correlation between the Southern Oscillation Index (SOI) and the precipitation during El Niño, La Niña, and neutral years (Fig. 9). The First pattern is similar to the temporal correlation between the SOI and the spatial distribution of precipitation during the 2001-2002 neutral years. The second spatial EOF reproduces the El Niño association between SOI and the 1997-98 precipitation pattern. The temporal variation of these patterns also shows the 2002-2003 and 2004 El Niño events. The third spatial EOF reproduces the patterns observed for La Niña of 1998-1999.

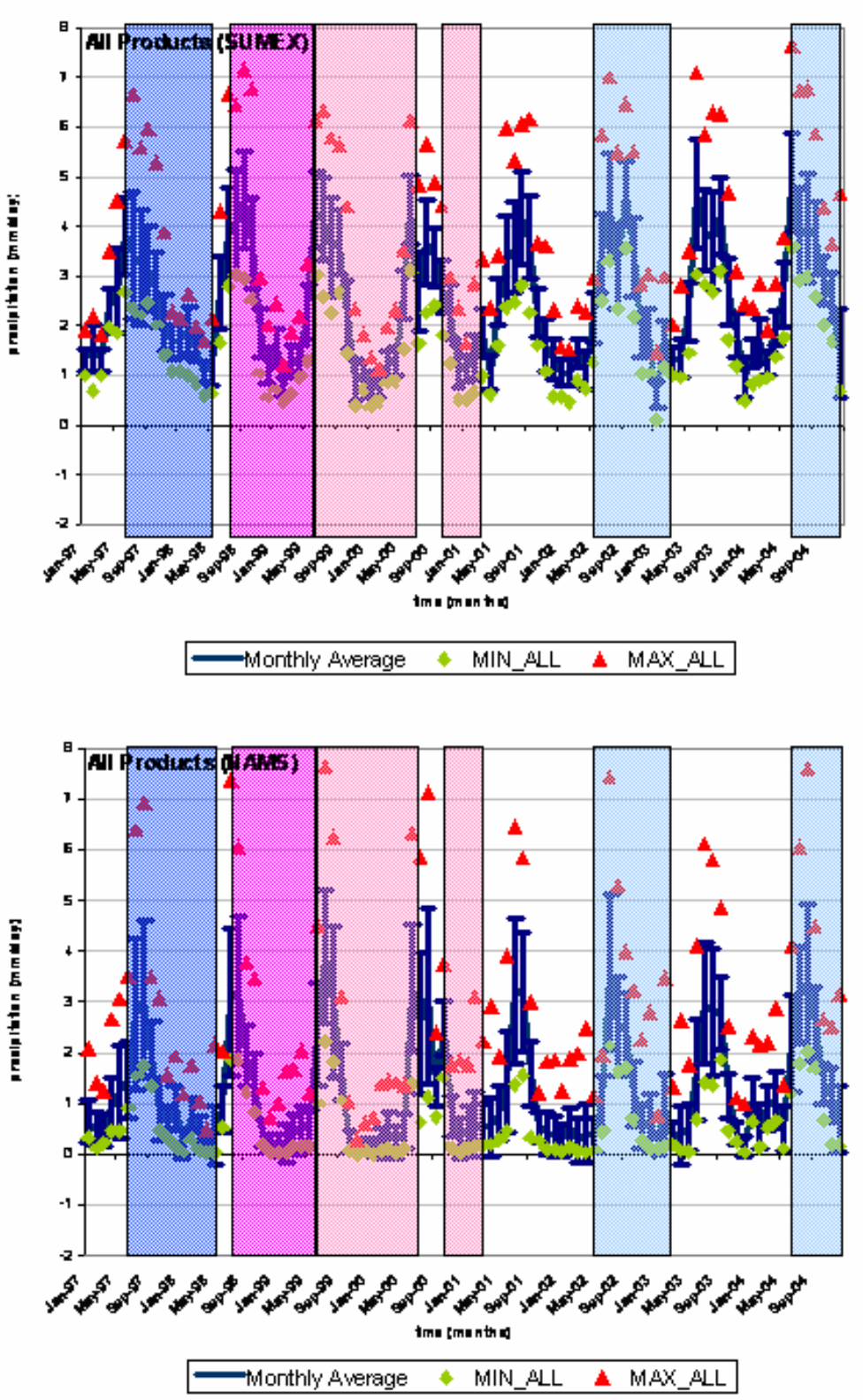

Figure 7: *Temporal variability of precipitation in SUMEX (top) and NAM (bottom) obtained from all datasets (n=18).*

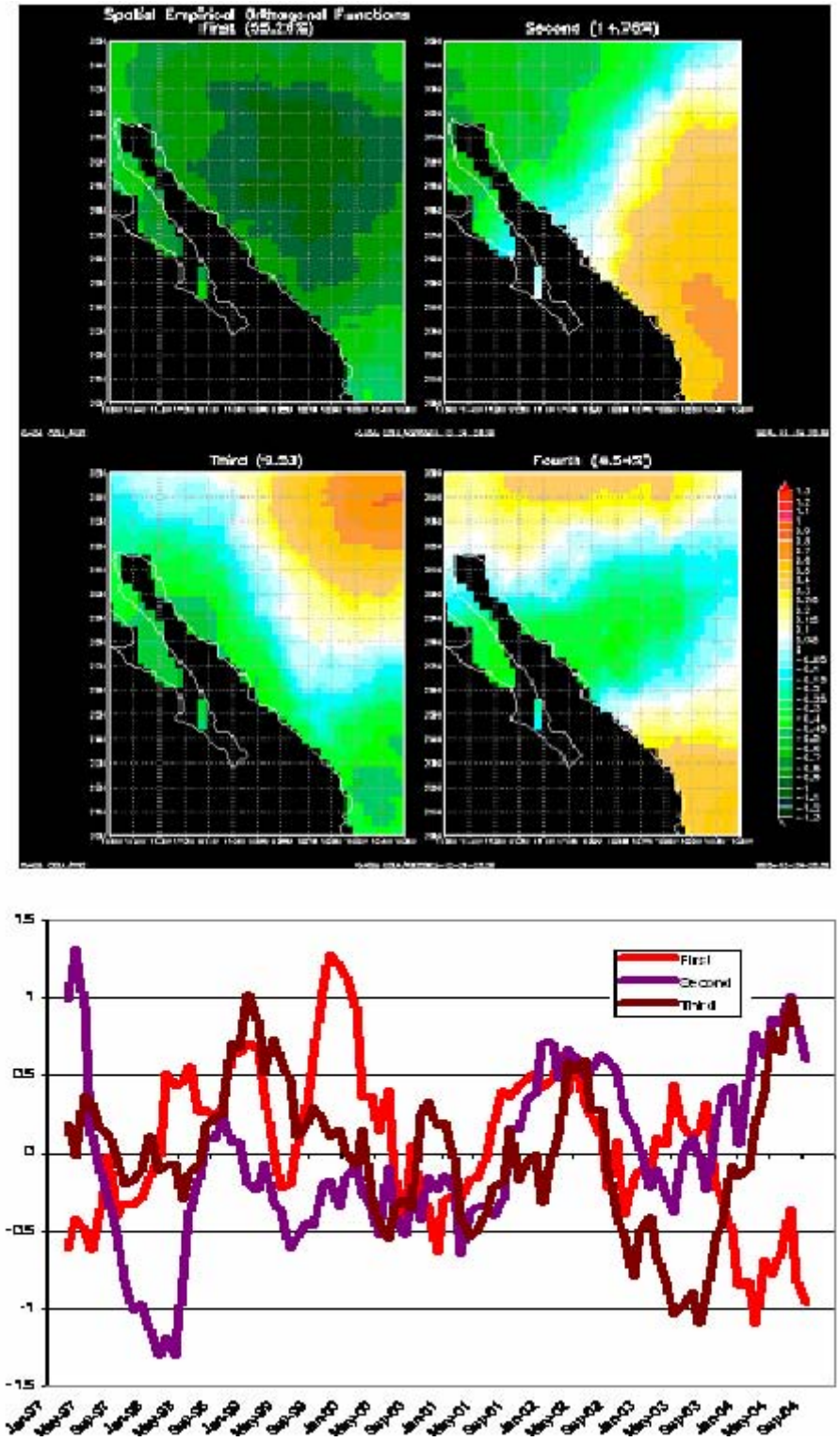

Figure 8: *Spatial (top) and temporal (bottom) Empirical Orthogonal Functions obtained from all datasets (n=18).*

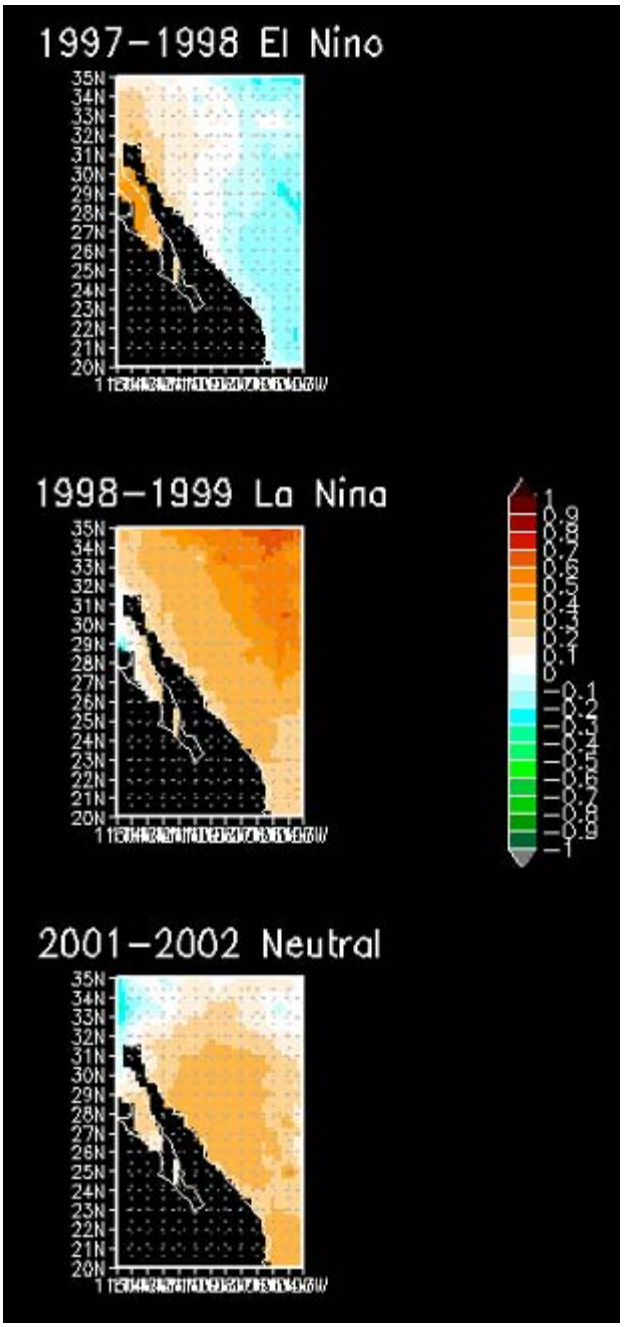

Figure 8: *Correlation coefficient between the Southern Oscillation Index and precipitation for El Nino (top) La Nina (middle) and neutral (bottom) years obtained from all datasets (n=18).*

b. Modeling:

We use the Regional Atmospheric Modeling System Version 6.0 (hereafter referred to as RAMS-6.0) for our experiments. During this past year, we have used this model at various resolutions to evaluate its performance as well as to emphasize the benefits of high-resolution modeling of precipitation in the NAME region. The NCEP-DOE AMIP II

Reanalyses are used to provide initial and dynamic lateral boundary conditions for RAMS-6.0. The Land-Ecosystem-Atmosphere Feedback 3 (LEAF-3) model provides the land-surface boundary conditions.

As a first experiment, we designed a horizontal domain of 8000 km × 6208 km centered over the U.S. and discretized with uniform, rectangular, Cartesian grid with 64 km spacing. In the vertical, the domain is 24 km high. However, the vertical grid is non-uniform, starting with a 50 m spacing near the surface and vertically increasing with a stretch ratio of 1.2, till a maximum of 1500 m is reached. In the ADAP system, the vertical grid is rectangular Cartesian, while in the σ-system, the vertical levels are terrain-following. However, they are exactly identical if the topography is zero.

RAMS-6.0 offers two different subgrid-scale convection schemes: a generalized Kuo scheme (Molinari, 1985) and the Kain-Fritsch scheme (Kain, 2004). Both are equilibrium schemes where subgrid-scale convection acts to consume the convective instability created by resolved-scale processes. The major difference between them is in the closure assumptions; Kuo being based on moisture convergence while Kain-Fritsch on convective available potential energy.

We performed 4 simulations by combining 2 coordinate systems and 2 convection schemes. In each case, the model was run for the entire month of July 2004. Figure 9 compares the simulated accumulated precipitation in the 4 experiments with observations from CPC U.S. and Mexican daily precipitation analysis at 0.25° resolution. All 4 simulations successfully capture the same broad patterns: high rainfall along the west coast of Mexico and the east coast of the U.S. and very low rainfall west of the Rockies. However, due to the coarse resolution, the simulations fail to adequately capture the finer structures visible in the analysis data. In this context it should be noted that the high precipitation zones along the model domain boundaries are artifacts of nudging and not produced by any physical process.

Despite the broad similarities, significant differences exist between the precipitation simulated by the 4 experiments. The Kain-Fritsch with ADAP run is closest to the analysis in terms of both spatial pattern and magnitude of precipitation. The major difference is that it generates excess rain in the Pacific Northwest and not enough in Florida. The Kain-Fritsch with Sigma run produces excessive rain in Mexico and the Great Plains. Both Kuo experiments produce localized hotspots of intense rainfall. In order to identify the physical process underlying these differences, we look at the contribution of vertical velocity (w). This is an important variable because a highly-resolved vertical velocity often indicates horizontal mass convergence and large-scale instability.

The question that needs to be answered is: can differences in w between two experiments explain the differences in precipitation simulated by those experiments? To answer this we define two variables:

$\Delta w = w_\sigma - w_C$

and

$\Delta P = P_\sigma - P_C$

where *w* is the vertical velocity (m/s), *P* is precipitation rate (mm liquid equivalent/hr) and the σ and C subscripts refer to the coordinate systems used in the experiments. We compute these quantities at each grid cell and correlate the two.

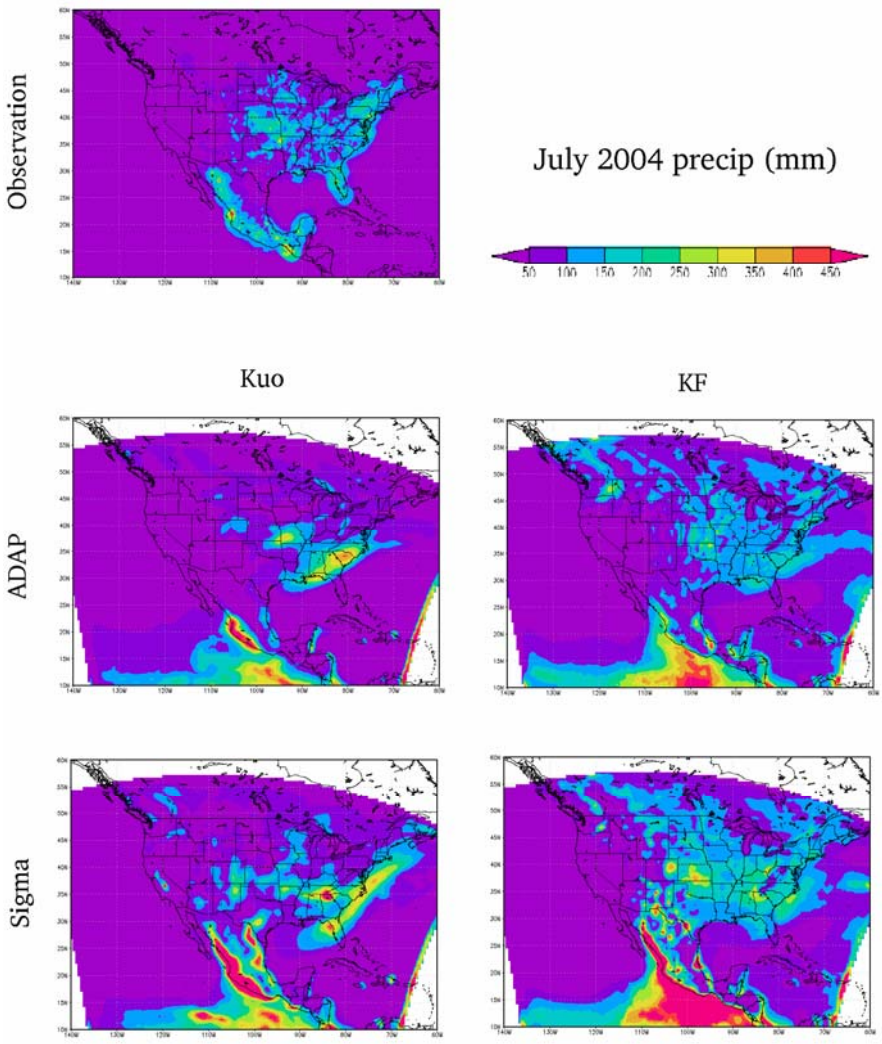

Figure 9: *Accumulated precipitation (mm) for July 2004. The top left panel shows observations from the U.S. and Mexican daily precipitation analysis at 0.25° spatial resolution. The other 4 panels show preliminary simulation results for Kuo with ADAP (middle left) and Sigma (bottom left) and Kain Fritsch with ADAP (middle right) and Sigma (bottom right).*

Figure 10 shows the results of the analysis for two levels. At 2200 m the correlation in both cases is strongly positive, especially in the Kuo case where most of the land regions exhibit a correlation higher than 0.6. In the Kuo scheme *w* plays an important role: *w* at the Lifting Condensation Level, typically between 2-3 km, acts as the trigger that initiates convection. In the Kain-Fritsch scheme the link is weaker: *w* at the LCL is used to compute a temperature perturbation, which is added to the parcel temperature at the LCL.

However, at 567 m (typical mid-day PBL height) the correlation is relatively weak implying that most convective cells do not grow to deep convection scale.

These results show that momentum transport is important for simulating precipitation. These results are preliminary. Currently we are investigating why ADAP produces more realistic *w* than Sigma.

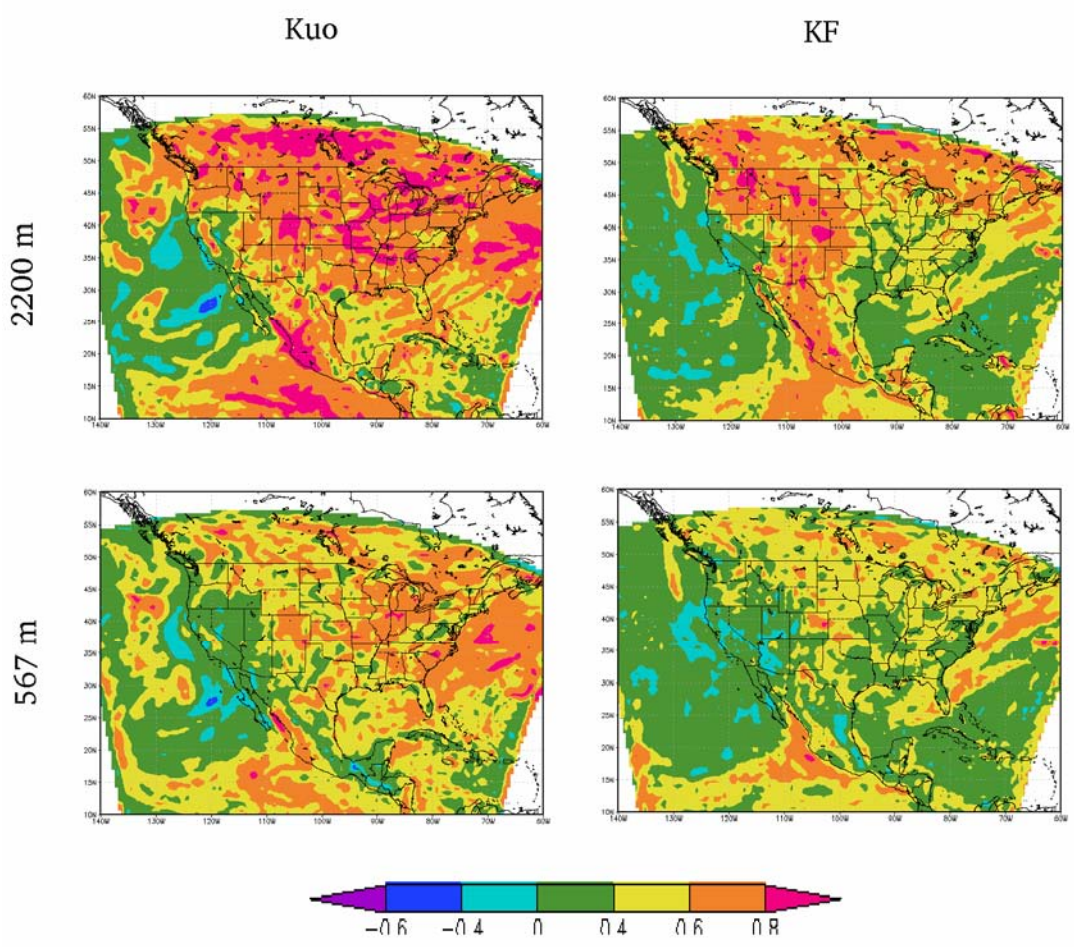

Figure 10: *Correlation of vertical velocity (w) difference and precipitation rate difference between sigma and ADAP runs. At each grid cell, instantaneous w in ADAP run was subtracted from instantaneous w in Sigma run. This difference was correlated with difference in precipitation rate for that grid cell. The left column represents the Kuo runs and the left column is for Kain-Fritsch runs. This analysis was performed with w from several vertical levels. The top row is for w at 2200 m while the bottom row is for 567 m.*

Following these initial, low-resolution simulations, we also started to produce very-high resolution simulations. For this purpose, the model domain consisted of 3 nested grids in the horizontal:

Grid #	# of points	Size	dx=dy	dt
Grid 1	102 x 102	3232 km x 3232 km	32 km	45s
Grid 2	202 x 202	1608 km x 1608 km	8 km	15s
Grid 3	302 x 302	604 km x 604 km	2 km	5s

The finest grid (24-30N latitude, 113-107W longitude) covered more than half of the observed continental core of the NAM. The vertical domain was 24 km high and discretized with a stretched grid starting from 50 m at the surface to a maximum of 1500 m aloft, with a stretch ratio of 1.2. Kain-Fritsch convection scheme was used in the coarse grid while the two finer grids explicitly resolved convection.

Using this setup we conducted a series of sensitivity studies to identify which parameters are crucial in improving precipitation simulation for the NAM. In this context, we focused on the comparative performance of the ADAP and sigma coordinate systems as well as various TKE formulations. Only outputs from the finest grid were used for our analysis.

In this configuration, a simulation requires more than 800 MB of RAM and 2.1E-05 s of wall time per grid cell per time step. A month-long simulation takes about 16-17 days real time when run in parallel on 24 nodes (at this rate, a month-long simulation with a 1 km horizontal grid will require more than 3 GB of RAM and about 100 days real time).

Figure 11 shows the observed and simulated precipitation in the NAM region for 15 days – July 1-15, 2004. The model successfully captured the north-west progression of the monsoon with high precipitation zones over elevated terrain. Both ADAP and sigma coordinate runs significantly overestimated rainfall. However, the sigma coordinate run produced about 15% more rainfall than the ADAP run. Comparing the dynamics prior to precipitation events, we found that the model generated unusually large amount of TKE at high elevations. This is evident in Fig. 12 where the model generated more than 40 m^2/s^2 TKE between 3000 and 6000 m elevations prior to an intense precipitation event. The Mellor-Yamada scheme is a robust TKE scheme and appropriate for the grid spacing used in our experiments. However, this scheme is meant for turbulence in the planetary boundary layer and may not be suitable for representing turbulence in upper atmosphere. The mixing lengthscale in this method is proportional to the height above ground. For elevated locations, this quantity is large and at times leads to an overestimation of TKE. We experimented with several modifications to the TKE scheme. Figure 13 shows the results of these experiments. Assuming that turbulence above 4000 m is purely local, we set the lengthscale to the vertical grid-spacing (dz) in those regions. However, in this case, turbulent transport was reduced but that was balanced by an increase in resolved transport, resulting in a significant increase in rainfall. In another experiment, we capped the TKE at elevations higher than 4000 m to a maximum value of 5 m^2/s^2. While this

improved the rainfall simulation, this purely empirical approach is not theoretically justified. In our experiments, TKE plays a significant role: Mixing coefficients for turbulent transport of momentum and scalars are based on TKE. Accurate estimation of TKE is essential for proper simulation of vertical moisture transport, which will lead to better representation of cloud-formation and precipitation processes. Currently, we are experimenting with improving the representation of TKE in our model.

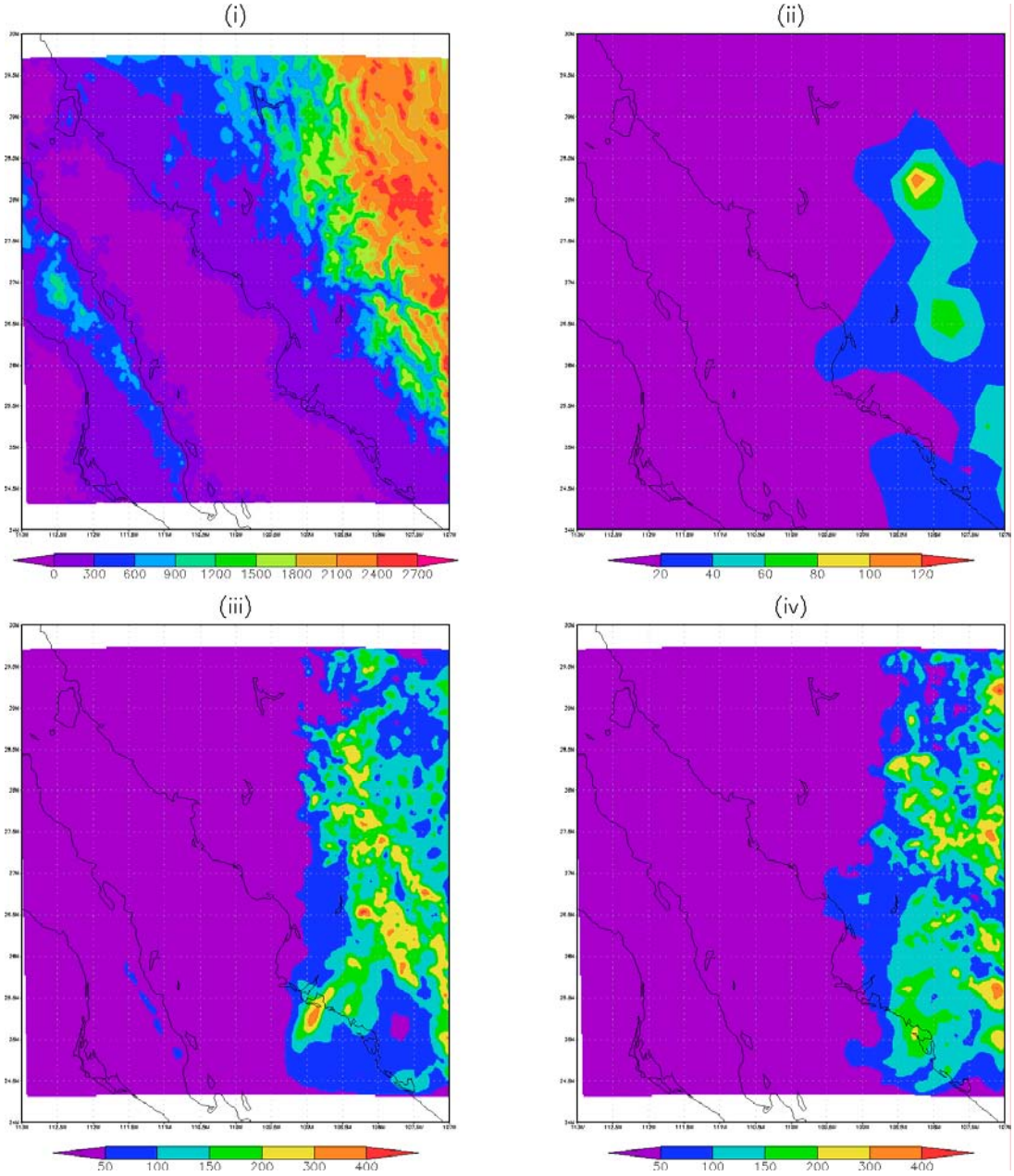

Figure 11: *(i) Topography (m) in the finest grid, (ii) observed precipitation (mm) for July 1-15, 2004, from the 0.25 x 0.25 degree daily US & Mexican precipitation analysis, and simulated precipitation (mm) for the same period using the (iii) sigma and (iv) ADAP coordinate systems.*

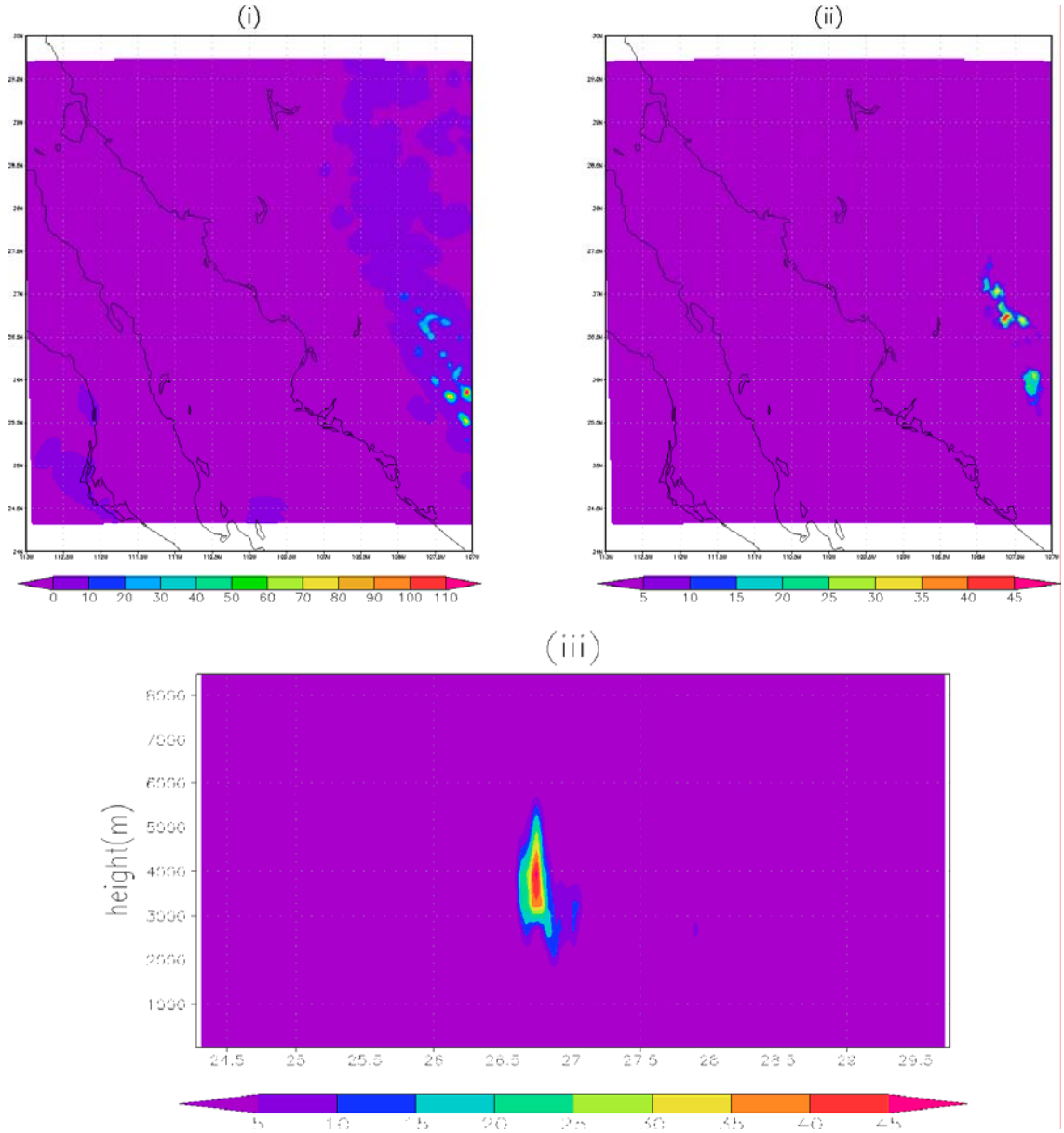

Figure 12: *(i) Simulated precipitation (mm) for a 2 hour period (July 1, 22 UTC - July 2, 00 UTC), TKE (m^2/s^2) on July 1, 22 UTC for (ii) a horizontal cross-scetion 4000 m above ground and (iii) a vertical cross-section along 107.6 W longitude.*

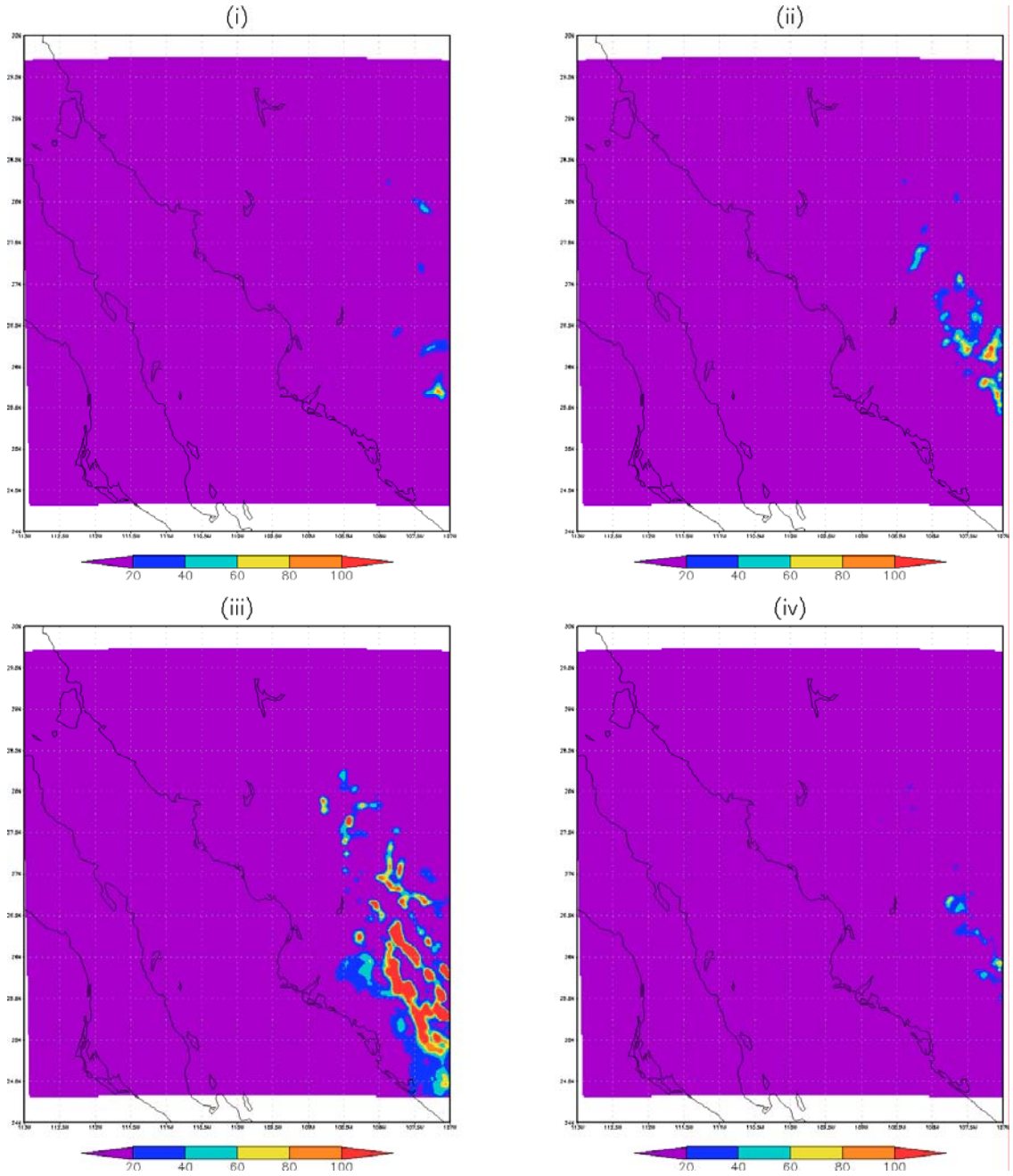

Figure 13: *Simulated precipitation (mm) for July 1-6, 2004, with (i) ADAP and sigma coordinate system with different modifications in the Mellor-Yamada TKE schemes -- (ii) lengthscale = height above ground, (iii) lengthscale = height above ground for elevations below 4000 m & lengthscale = dz otherwise (iii) TKE capped at 5 m^2/s^2 at heights 4000 m and above.*

References:

Adler, R.F., G. J. Huffman, A. Chang, R. Ferraro, P. Xie, J. Janowiak, B. Rudolf, U. Schneider, S. Curtis, D. Bolvin, A. Gruber, J. Susskind, P. Arkin, and E. Nelkin, 2003: The Version-2 Global Precipitation Climatology Project (GPCP) Monthly Precipitation Analysis (1979-Present). *J. Hydrometeor*., **4**, 1147-1167.

Arkin, P.A., and B.N. Meisner, 1987: The Relationship between Large-Scale Convective Rainfall and Cold Cloud over the Western Hemisphere during 1982-84. *Mon. Wea. Rev*., **115**, 51-74.

Beeson. P.C., S. N. Martens and D. D Breshears (2001). Simulating overland flow following wildfire: mapping vulnerability to landscape disturbance. Hydrological Processes. 15: 2917-2930.

Beven K.J. and M.J. Kirkby (1979). A physically based, cariable contributing area model of basin hydrology. Hyydrological Sciences-des Sciences Hydrologiques, 24(1):43-69.

Beven, K., R. Lamb, P. Quin, R. Ramanowics, and J Freer (1995). TOPMODEL. Computer Models of Watershed Hydrology, In: Singh, V.P (Ed) Computer Models of Watersheed Hydrology, pp., 627.

Beven, K. and Freer, J. (2001b). A dynamic TOPMODEL. Hydrological Processes, 15(10): 1993-2011.

Beven, K., J.Freer, B.Hankin, and K. Schulz (2002). The Use of a Generalized Likelihood Measures for Uncertainty Estimation in High-Order Models of Environmental Systems. In: Fitzgerald, W.J., R.L. Smith, A.T. Walden, and P. Young (Eds.) Nonlinear and Nonstationary Signal Processing, pp.115-151.

Burnash, R.J.C., (1995). The NWS River Forecast System in Catchment Modeling, Computer Models of Watershed Hydrology, In: Singh, V.P (Ed) Computer Models of Watersheed Hydrology,. pp. 311-366.Ferraro, R.R., 1997. Special sensor microwave imager derived global rainfall estimates for climatological applications. Journal of Geophysical Research-Atmospheres, 102(D14): 16715-16735.

Ferraro, R. and Q. Li, (2002). Detailed analysis of the error associated with the rainfall retrieved by the NOAA/NESDIS Special Sensor Microwave/Imager algorithm 2. Rainfall over land, Journal of Geophysical Research., 107(D23), 4680, doi:1029/2001JD001172, 2002.

Franz, K.J., Hartmann, H.C., Sorooshian, S. and Bales, R. (2003). Verification of national weather service ensemble streamflow predictions for water supply forecasting in the Colorado River basin. *J. Hydrometeorol.,* 4(6): 1105-1118.

Gruber, A., X. Su, M. Kanamitsu, and J. Schemm (2000). The comparision of two merged rain gauge-satellite precipitation datasets. Bulletin of the American Meteorological Society, 81(11): 2631-2644.

Gutowski, W. J. et al., (2002). A coupled land-Atmosphere Simulation Program (CLASP): Calibration and Validation. *J. Geophys. Res.*, 107(D16): ACL 3-1-3-17.

Huffman, G. J., R.F. Adler, B. Rudolf, U. Schneider, and P.R. Keehn (1995) Global precipitation estimates based on a technique of combining satellite-based estimates, rain gauge analysis, and NWP model precipitation information. Journal of Climate, 8, 1284-1295.

Huffman, G.J. R.F. Adler, P. Arkin, A. Chang, R. Ferraro, A. Gruber, J. Janowiak, A.McNab, B. Rudolf, and Udo Schneider 1997. The Global Precipitation Climatology Project (GPCP) Combined Precipitation Dataset. Bulletin of the American Meteorological Society, 78(1): 5-20.

Hulme, M., 1992. A 1951-80 Global Land Precipitation Climatology for the Evaluation of General-Circulation Models. Climate Dynamics, 7(2): 57-72.

Hulme, M. (1994). Validation of large-scale precipitation fields in GCMs. In: Global Precipitations and Climate Change (Eds. Desbois, M and F. Désalmand, F.): 387-406.

INEGI (1993). Estudio Hidrológico del Estado de Sonora. Instituto Nacional de Estadística Geografía e Informática.

Kummerow, C. et al., 2000. The status of the Tropical Rainfall Measuring Mission (TRMM) after two years in orbit. Journal of Applied Meteorology, 39(12): 1965-1982.

Kummerow, C. et al., 2001. The evolution of the Goddard profiling algorithm (GPROF) for rainfall estimation from passive microwave sensors. Journal of Applied Meteorology, 40(11): 1801-1820.

Liang, X., Lettenmaier, D.P. and Wood, E.F. (1996). One-dimensional statistical dynamic representation of subgrid spatial variability of precipitation in the two-layer variable infiltration capacity model. *J. Geophys. Res.*, 101(D16): 21403-21422.

Liang, X., Lettenmaier, D.P., Wood, E.F. and Burges, S.J. (1994). A Simple Hydrologically Based Model of Land-Surface Water and Energy Fluxes for General-Circulation Models. *J. Geophys. Res.*, 99(D7): 14415-14428.

Martin, K. (2002) NWSRFS calibration parameter selection and Geologic Reasoning: Pacific northwest cases. *J. Amer. Water Res. Association*, 38(5): 1349-1362.

McCollum, J.R., W.F. Krajewski, R.R. Ferraro, and M.B. Ba (2002). Evaluation of biases of satellite rainfall estimation algorithms over the continental United States, Journal of Applied Meteorology, 41: 1065-1080.

Simpson, J., Adler, R.F. and North, G.R., 1988. A Proposed Tropical Rainfall Measuring Mission (Trmm) Satellite. Bulletin of the American Meteorological Society, 69(3): 278-295.

Willmott, C.J., S.M. Robertson and J.J. Freddema, (1994). Estimating continental and terrestrial precipitation averages from rain-gauge networks. International Journal of Climatology. 14(4): 403-414.

Willmott, C.J. and K. Matsuura, (2000). http://climate.geog.udel.edu/~climate/html_pages /README.ghcn_clim.html.

Xie, P.P. and Arkin, P.A., 1996. Analyses of global monthly precipitation using gauge observations, satellite estimates, and numerical model predictions. Journal of Climate, 9(4): 840-858.

Xie, P.P. and Arkin, P.A., 1997. Global precipitation: A 17-year monthly analysis based on gauge observations, satellite estimates, and numerical model outputs. Bulletin of the American Meteorological Society, 78(11): 2539-2558.

Yu, Z, (2000). Assessing the response of subgrid hydrologic processes to atmospheric forcing with a hydrologic model system. *Global and Planetary Change*. 25: 1-17.

Yu, Z, and F. W. Schwartz, (1999). Automated calibration applied to watershed-scale flow simulations. *Hydrological Processes*. 13: 191-209.

Yu, Z, M.N. Lakhtakia, and E.J. Barron, (1999). Modeling the river-basin response to single-storm events simulated by a mesoscale meteorological model at various resolutions. *J. Geophys. Res.*, 104 (16): 19675-19689.

Future Work (Year 3: 04/01/2006 – 03/31/2007):

We are progressing with our plan as established in our original proposal. This year, we will finalize the production of a very-high resolution precipitation dataset with RAMS-6.0, which together with other sources of precipitation data will be used to force the VIC hydrology model applied to the three river basins that we have selected in the NAME region. This combination of data sources and model runs will provide a “super ensemble” that will be used to assess the impact of land-cover change in that region.

Contacts:

Principal Investigator Name: Roni Avissar
E-mail: avissar@duke.edu
Phone: 919 660-5458
Fax: 919 660-5459
Institution Name: Duke University – Department of Civil and Environmental Engineering
Address: 123 Hudson Hall, Box 90287, Durham, NC 27708-0287
Web Link; http://www.cee.duke.edu